# Optimization of the surface properties of nanostructured Ni–W alloys on steel by a mixed silane layer

M.P. Quiroga Argañaraz[1], J. M.Ramallo-López[1], G.Benítez[1], A.Rubert[1], E.D.Prieto[1], L.M.Gassa[1], R.C.Salvarezza[1], M.E.Vela*,[1]

[1]Instituto de Investigaciones Fisicoquímicas Teóricas y Aplicadas (INIFTA), Universidad Nacional de La Plata - CONICET- Sucursal 4 Casilla de Correo 16, (1900) La Plata, Argentina.

**Keywords: Ni–W alloys, nanostructured surfaces, silanes, corrosion protection, wetting.**

## Abstract

Ni–W nanostructured coatings electrodeposited on steel by galvanostatic pulses were functionalized by tetraethoxysilane (TEOS) and octadecyltrichlorosilane (OTS) in a two-step procedure. A silica-rich layer is formed by the reaction of TEOS with the metal coating surface oxides, which allows a further reaction with OTS forming a hydrocarbon-silica outer network. This mixed silane layer provides hydrophobicity and improves the corrosion behavior of the Ni–W surface coatings without modifying their excellent mechanical properties

*Corresponding author:

María Elena Vela
Address: INIFTA. Diagonal 113 esquina 64. CC 16 Suc 4 (1900) La Plata. ARGENTINA. TE +54 221 4257430, FAX: +54 221 4254642
E-mail: mevela@inifta.unlp.edu.ar

## Introduction

The wide variety of technological applications of steels has led to the search of different procedures to increase their protection, to obtain improvements in their mechanical performance and to tailor their properties to specific demands. Among the diversity of strategies, the electrodeposition of metallic alloys is one of the most extensively used when hardness and corrosion resistance is required.

Nickel–tungsten (Ni–W) coatings electrodeposited on metallic substrates allow the simultaneous deposition of both Ni and W, controlling the composition of each component through the electrochemical potential, current density and the chemical composition of the electrolytic solution.[1-4] These variables also allow adjusting the grain size in the nanometric range in a way that improved mechanical properties and good corrosion resistance are achieved.[5-13] In the field of catalysis, Ni–W alloys are promising materials for the hydrogen evolution reaction.[14-16]

In order to optimize interfacial properties and/or search for special applications of metallic coatings, the strategy of functionalization with self-assembled mono or multilayers appears as the simplest procedure.[17-19] Silanes or phosphonates are suitable compounds for those metallic surfaces that are spontaneously covered by their oxides such us Ti, Al, Hf, Zn, Sn, Mg alloys, steel and Ni alloys. [18,20-30] The terminal OH groups of the oxihydroxide metallic surface react with silanes that undergo hydrolysis forming polysiloxane (Si–O–Si) bonds and Si–O–substrate bonds.[31,32] The formation of a robust bond of the silanes with the substrate confers a strong stability to the layer and allows further chemical functionalization.[33] Although the best substrates for silane functionalization are those containing Si–OH moieties, metallic oxides are also suitable. Silanization can be carried out either by dip-coating procedures or from vapors in a controlled atmosphere. [31,34-38] The first step consists in the reaction of silane with water

adsorbed at the surface oxides forming silanol groups. When silanes are used as coupling agents they should form a stable bond with another organic or inorganic material that would react forming a mixed silane layer. A wide variety of chemical strategies can be implemented according to specific applications.[39,40] In the field of corrosion protection, the inhibition efficiency is attributed to the hydrophobicity of the silane layer.[24,41] Crosslinking processes that occur at higher temperatures improve the corrosion performance of the protective film.[42]

In this work we propose a two-step functionalization method for nanocrystalline Ni–W alloy coatings combining the ability of TEOS to form an adhesive layer with the metallic substrate, which then reacts with OTS to confer hydrophobic character to the film. The mixed silane layer provides high hydrophobicity and corrosion protection preserving the hardness of the Ni–W coating.

**Experimental**

Nanocrystalline Ni–W coatings were deposited on carbon steel (SAE 1020) sheets (area = 1 cm$^2$) which were previously polished with grit paper and alumina powder. The electrodeposited coatings were obtained galvanostatically by pulse electroplating ($\tau = \tau_{on} = \tau_{off} = 5$ ms) using an Autolab 128N using a cathodic current of 140 mA cm$^{-2}$ and zero current during 60 min. The maximum film thickness was $\approx 40$ μm.[10]

The plating bath contained 0.06 M NiSO$_4$.6H$_2$O, 0.14 M Na$_2$WO$_4$.2H$_2$O, 0.5 M Na$_3$C$_6$H$_5$O$_7$.2H$_2$O, 0.5 M NH$_4$Cl and 0.15 M NaBr (pH = 9.5). A fresh plating bath was prepared for each experiment using pure chemical reagents and Milli-Q H$_2$O (18 MOhm cm). It has been reported that this bath produces amorphous and nanocrystalline Ni–W alloys having high hardness and good ductility. [2,10] The solution was gently stirred during the plating at 65 ºC and degassed with purified nitrogen.

The silanization procedure was carried out on clean Ni–W substrates that were ultrasonicated in acetone during 10 min. The samples were dipped in the solution containing approximately 20 ml of 2 mM tetraethoxysilane (TEOS) solution in toluene at 80ºC for 3 h. After the immersion, the samples were washed for 10 min by immersion in toluene and immediately dipped in a second solution containing 20 ml of 7 mM octadecyltrichlorosilane (OTS) in hexane for 24 h. Finally the substrates were rinsed in hexane to remove loosely bound materials and subsequently air dried.

The surface composition was evaluated by XPS using an Al K$\alpha$ source (1486.6 eV) XR50, Specs GmbH, and a hemispherical electron energy analyzer PHOIBOS 100, Specs GmbH.

Static contact angle (CA) characterizations were carried out with a Ramé-Hart goniometer (model 500, Netcong, NJ) with water as the probe liquid. Measurements were performed on at least three different points to calculate the average static CA.

FTIR spectra were acquired with an FTIR Nicolet 380 spectrophotometer, ATR mode (64 scans and a resolution of 2 cm$^{-1}$).

Surface topography was imaged with contact AFM under ambient conditions using a MultiMode Scanning Probe Microscope (Veeco, Santa Barbara, CA. USA) equipped with a Nanoscope V controller. All the measurements were performed using contact sharpened silicon nitride probes (DNP –S10, Bruker) with nominal tip radius of 10 nm.

Microhardness measurements were carried out with a FUTURE-TECH micro–indenter. The measurements were performed on samples cross-sections applying a load of 10 g for 10 s. Nanohardness was evaluated using a Triboindenter TI series 900, Hysitron Inc. MN, USA with a diamond indenter tip.

To evaluate the corrosion resistance of the Ni–W coatings with and without silanization, a single triangular potential sweep (STPS) between preset cathodic ($E_{s,c}$)

and anodic ($E_{s,a}$) switching potentials, at a potential scan rate (v) in the $0.002 \text{ V s}^{-1} \leq \text{v} \leq$ $0.025 \text{ V s}^{-1}$ range, and anodic polarization curves obtained at a low scan rate ($2 \text{ mV s}^{-1}$) were applied in a still phosphate–borate buffer ($0.1 \text{ M KH}_2\text{PO}_4 + 0.05 \text{ M Na}_2\text{B}_4\text{O}_7$) pH 8.00, with the addition of $1 \text{ M Na}_2\text{SO}_4$ in the same solution. The sulfate ion becomes more aggressive than the chloride ion in neutral and alkaline solutions, causing pitting.[43,44] A standard three–electrode cell with a large area Pt sheet counter electrode and a saturated calomel reference electrode (SCE) were used. All potentials in the text were referred to the SCE (0.241 V vs SHE). Experiments were made under purified $N_2$ gas saturation at 25 °C. Evolution of the open circuit potential (OCP) with time was followed for Ni–W without functionalization and with TEOS and TEOS&OTS in non–deaerated phosphate–borate solution containing $\text{Na}_2\text{SO}_4$ 1M.

**Results and Discussion**

Figures 1a-c shows the XPS data for the electrodeposited Ni–W surface. These data reveal that Ni and W are present on the surface in the metallic state and also as their corresponding oxides: NiO, and NiOOH for Ni, and $WO_3$ for W (Figure 1b,c). The Carbon signal is also evident in the spectra, a fact that can be assigned to the adsorption of citrate anions present in the plating bath on the oxide layer.[45] It is interesting to note that Fe is not present in these spectra indicating that the Ni–W coating entirely covers the steel substrate surface.

The complex Ni and W oxide layer is suitable for silanization since the nickel and tungsten oxyhydroxides can react with the alkoxy groups of TEOS in the first step of the functionalization forming covalent Si–O–metal and Si–O–Si bonds that constitute the platform for the post-functionalization with OTS. This strategy has been previously used to improve the adhesion and corrosion resistance of single-silane layers on different substrates.[46]
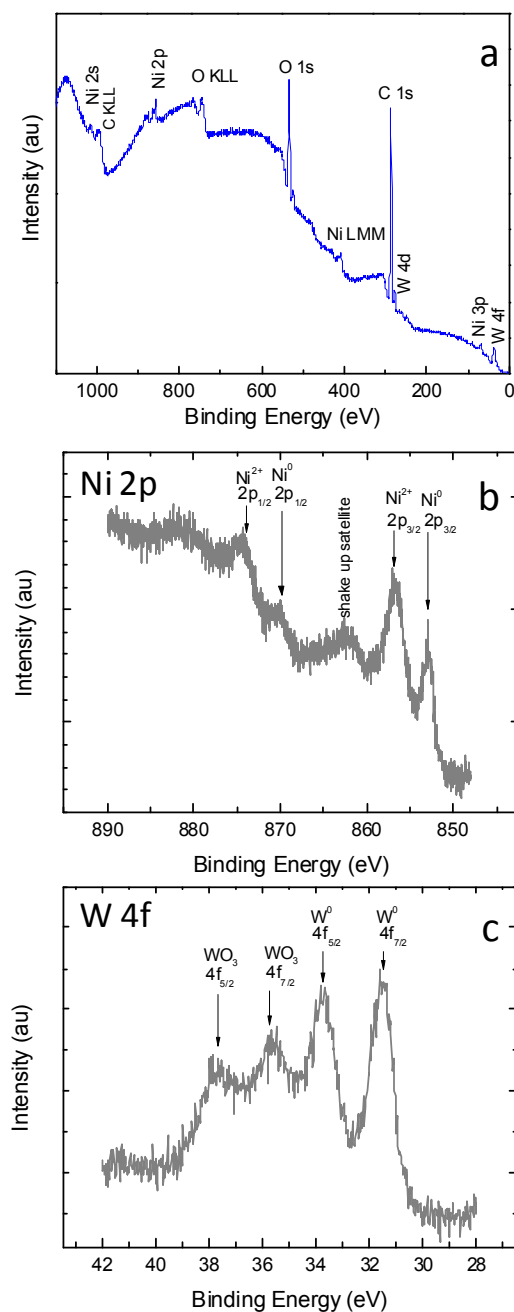
*Figure 1. a) XPS survey of Ni–W electrodeposited on carbon steel, b) Ni 2p region, c) W 4f region.*

Therefore, the first step was the immersion of the Ni–W coating steel substrate in the TEOS-containing toluene solution at 80°C to form a silica-rich layer on the surface. After this treatment, XPS data reveal a decrease in the Ni and W signals with respect to the untreated sample, while the Si signal is now visible in the spectrum with a Si/Ni

ratio ≈ 0.2 (Figure 2.a). The Si 2p peak can be fitted with a doublet with Si $2p_{3/2}$ at 102.6 eV, spin-orbit splitting of 0.6 eV and full width at half maximum (FWHM) 1.4 eV. This position can be assigned to Si-O-Si, Si-OH or Si-O-metal bonds.[47,48]
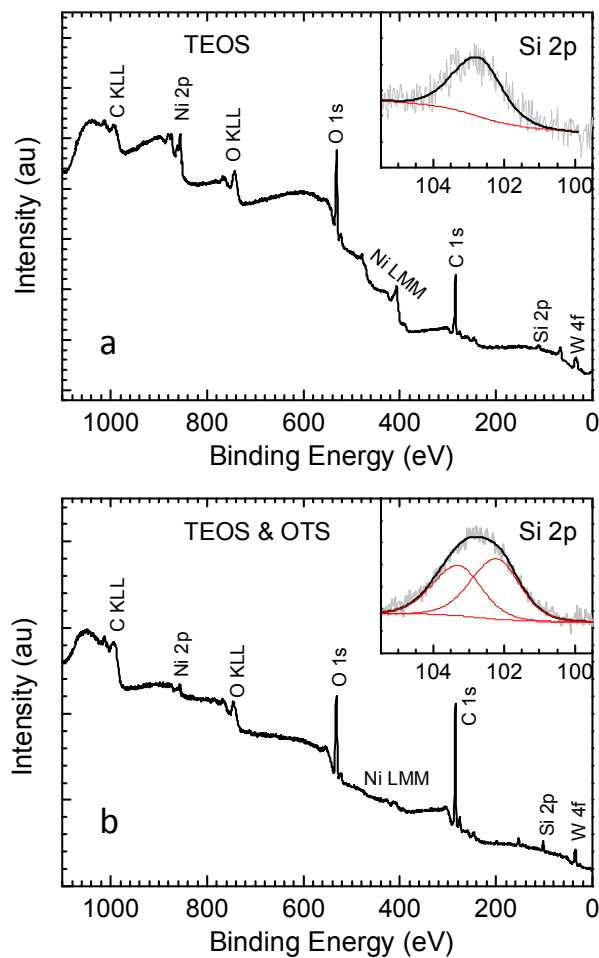


*Figure 2. XPS survey spectra of Ni–W electrodeposited on carbon steel after silanization with TEOS (a) and TEOS +OTS ( b). The insets show the Si 2p region.*

Static water contact angle measurements give θ ≈ 91° indicating a slight improvement of the hydrophobicity in relation to the bare Ni–W surface that exhibits θ ≈ 75° (Figure 3). Note that when the as-prepared electrodeposited Ni–W coating sample is sputtered with Ar the contact angle is 53°, indicating that the removal of the outer C compounds at the surface makes the more hydrophilic nickel and tungsten oxides determine the wettability.
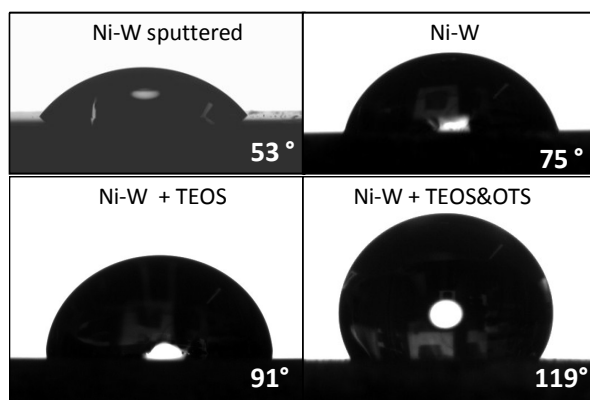
*Figure 3. Static water contact angle measurements for different Ni–W surfaces. The silanization procedure increases the hydrophobicity of the surface.*

In the second step the silica-rich Ni–W surface was immersed in the OTS containing hexane solution for 24 h. After this second treatment XPS data show that the Ni and W signals practically disappear in the spectrum, the O signal decreases and Si and C signals increase (Figure 2.b) with a Si/Ni ratio ≈ 8. In order to fit the Si 2p peak with the same FWHM (1.4 eV), a second doublet shifted 1.0 eV towards higher binding energies must be included. Whereas the peak at lower binding energies can be assigned to Si–O–Si and Si–OH bonds in the TEOS&OTS layer, the peak at 103.3 eV is probably due to a charging effect in the non-conductive polysiloxane layer. This shift is consistent with that observed in the C 1s region[49] (Fig. S1, Supporting Information).

The static water contact angle measurements on Ni–W coatings modified with TEOS&OTS Ni–W indicate that now the surface becomes highly hydrophobic with $\theta \approx$ 119° (Figure 3 bottom, right side). Nano and microscale roughness have been shown to affect the wettability.[50-52] Two factors are needed to create a superhydrophobic surface: low surface energy, a condition fulfilled for hydrophobic surfaces, and surface roughness.[52,53] For rough surfaces the contact angle of a liquid droplet with a rough surface is related to that with a flat surface by the Wenzel equation.[54] For heterogeneous interfaces the Cassie-Baxter equation applies.[55] Nevertheless, the

8

phenomena are not always described by those models. Some issues that should be clarified are the transition between the wetting states, stability of composite interfaces and a rigorous definition of the CA with heterogeneous surfaces among others.[53] In the TEOS&OTS Ni–W surfaces where a static contact angle of $\theta \approx 119°$ is obtained, we cannot ruled out that the nanometer roughness observed in our samples could have a role in the wettability of the surface. However, our experimental contact angle is in the order of those measured for OTS layers on solid substrates where typical values are 100-115°.[39,56-58] Thus, we interpret that in our system, the silica-rich surface formed after the TEOS treatment has been modified by the OTS molecules providing an outer hydrophobic layer by the alkyl chains.

The IR spectra of the TEOS&OTS Ni–W coatings are shown in Figure 4 and the assignments of the bands in Table 1. Two main bands at 2848 and 2915 $cm^{-1}$ can be related to the symmetric and antisymmetric $CH_2$ stretching.[59] The position of these maxima is an indication of the conformational order of the alkyl chains.[60,61] For totally disordered alkyl structures the $CH_2$ stretching band appears at values typical of liquid alkanes (2924 $cm^{-1}$) while for crystalline alkanes a value of 2915 $cm^{-1}$ is reported.[60,62] In the case of self-assembled monolayers frequencies lower than 2920 $cm^{-1}$ are characteristic of well ordered films with the alkyl chains in all-trans conformations while higher frequencies point to gauche defects and less ordered chains.[63] Finally, the minor peak observed at 2956 $cm^{-1}$ can be assigned to a $CH_3$ band.[31,64]. In the 1150–1300 $cm^{-1}$ range, a series of bands with a regular spacing of $\Delta\nu \cong 20$ $cm^{-1}$ are associated with a progression of coupled $CH_2$ wag modes[65] that usually appears in solid alkyl compound spectra with all-trans conformational sequences.[66] This value is close to $\Delta\nu \cong 18$ $cm^{-1}$ for an X-$(CH2)_{17}CH_3$ all-trans sequence, where X = SiOx.[61] The slightly higher $\Delta\nu$ spacing observed has been assigned to the presence of disorder in the last one or two $CH_2$

groups of the chain terminus at the ambient interface.[61,65] The crosslinking of silanes through the formation of Si–O–Si bonds was verified in the 1000–1150 cm$^{-1}$ spectral range.[61,67,68] These bonds are formed through the reaction of TEOS with the Ni–W hydrated oxides and in the second step when OTS reacts with terminal groups of TEOS and with neighboring OTS molecules forming a polysiloxane network.[68] A minor peak at 887 cm$^{-1}$ indicates that some Si–OH groups are not involved in the crosslinking.

**Table 1**

IR frequencies (cm$^{-1}$) for TEOS&OTS Ni–W on steel samples and their vibrational assignments

| Peak wavenumber(cm$^{-1}$) | Assignment | Reference |
|---|---|---|
| 720 | CH$_2$ rocking (T)* | [68] |
| 887 | Si-OH mode | [69] |
| 1020 | Si-O-Si antisymmetric stretching | [46,68] |
| 1103 | Si-O-Si antisymmetric stretching | [46,68] |
| 1150-1350 | CH$_2$ wag modes | [65,68] |
| 1465 | CH$_2$ scissoring | [65,68] |
| 2848 | CH$_2$ symmetric stretching | [65,68] |
| 2916 | CH$_2$ antisymmetric stretching | [65,68] |
| 2956 | CH$_3$ antisymmetric stretching | [65,68] |

\* T corresponds to trans–conformation of an alkyl chain.

Our results indicate that the two-step silanization produces a crystalline-like film as that observed previously for different silane precursors on metal oxides and silica beads. [63,68]
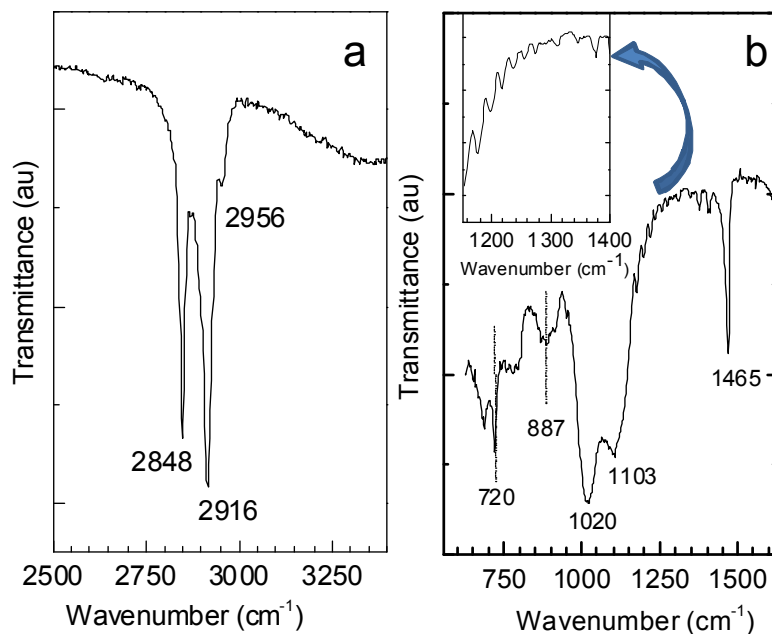
*Figure 4: IR–ATR spectra of TEOS&OTS Ni–W coatings in the C–H stretching mode region (a) and in the low wavenumber range where Si–O–Si bands are present (b). The inset corresponds to the $CH_2$ wag modes. Band assignments are explained in the text and in Table 1.*

Following accepted mechanisms for modification of surfaces with silanes[31] we propose that in the first step TEOS react with adsorbed water at the interface or Ni and W oxihydroxides (Figure 5a)  to form silanol groups. These silanols are capable to react with other silanols to form stable siloxane bonds (-Si-O-Si-) and also with the hydroxyl groups at the surface of the Ni-W coatings forming Si-O-Metal  bonds (Figure 5b).
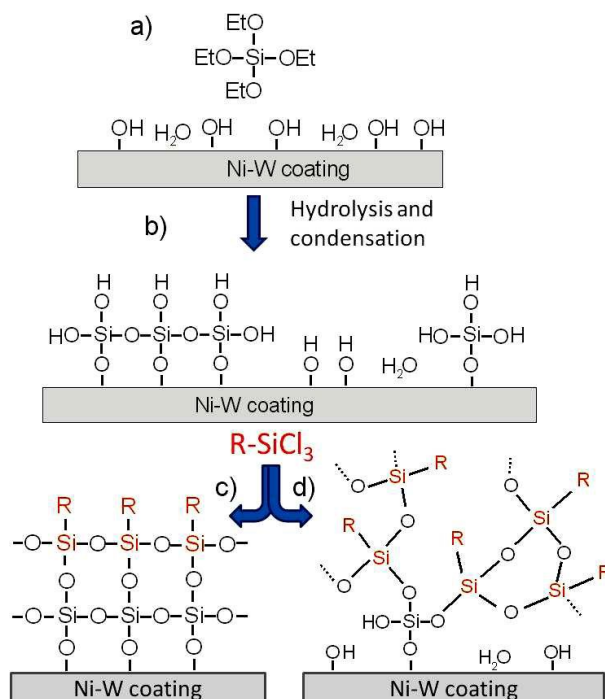
*Figure 5. Scheme of the proposed two-step mechanism for silanization with TEOS and OTS on Ni-W coatings. Et represents the ethyl group of TEOS and R is the octadecyl chain of OTS. a) TEOS molecules in the interface hydrolyze and/or condense to form siloxane bonds laterally and Si-O-metal bonds (b). OTS can react with the silanol groups of the first layer and with OH or water adsorbed at the interface forming ordered (c) or non-homogeneous multilayers (d).*

In the second step OTS molecules can react with the silanol groups formed previously by TEOS that act as coupling agents and/or with OH and adsorbed water in the interface. Octadecylsilanol groups can then condense in a laterally cross-linked structure (Figure 5 c) or can form non-homogeneous multilayers (Figure 5d). This situation would occur when in the first step TEOS molecules have not formed an homogeneous layer like the one depicted in Figure 5 b) left side, and many OH groups and adsorbed water are still available for reaction with OTS .

Regarding the mechanical properties, the electrodeposited Ni–W alloy coating exhibits excellent mechanical properties (600 HV microhardness, 1016 HV nanohardness). After the two-step functionalization procedure with TEOS&OTS the microhardness remains

unchanged whereas the nanohardness is 18 HV, a value that is expected for polymeric materials.[70]

The surface morphology of the TEOS&OTS Ni–W samples was studied by contact mode AFM microscopy (Figure 6a-b). The typical fractal cauliflower–like surface structure of the Ni–W alloy coating[10] is no longer visible after the functionalization and the root mean square roughness(rms) increases from 20 nm (Ni–W) up to 80–90 nm for TEOS&OTS Ni–W in 5x5 $\mu m^2$ images. The growth of the mixed silane film in our experimental conditions did not follow the Ni–W topography, as was checked in control experiments using mica as substrate (Fig. S2, Supporting Information) where the same silanization procedure was used. From this result one can infer that the polysiloxane layer follows its own topography after the early stages of film growth independently of the topography of the substrate where it grows.
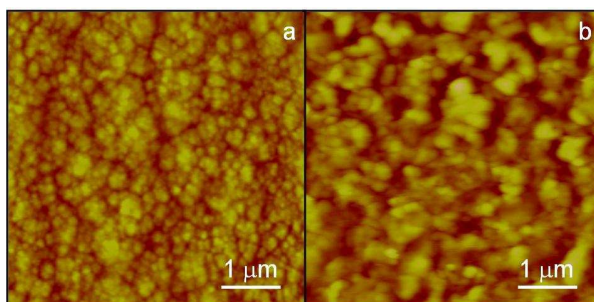


*Figure 6: 5μmx5μm AFM ex-situ images of a) Ni–W electrodeposited film. b) Ni–W modified with TEOS&OTS. The z color scale is the same in both images where brighter colors correspond to higher z values.*

The electrochemical behavior of the Ni–W coated steel and TEOS and TEOS&OTS functionalized Ni–W coated steel gives important information on the corrosion of the samples in aqueous media. First, we analyzed the anodic behavior of the samples that involves current densities (j) related to both oxide growth ($j_{ox}$) and metal electrodissolution ($j_{corr}$) through the oxide film. The j vs. applied potential (E) STPS profiles recorded at 0.025 V s$^{-1}$ in the anodic direction show that the functionalized

surfaces exhibit lower anodic j values than the bare Ni–W coated steel in the overall

potential range (Figure 7). This result indicates that the polysiloxane layer formed after

the TEOS and TEOS&OTS functionalization decreases water access and its adsorption

on the Ni–W surface, thus hindering the formation of the oxide film involved in the
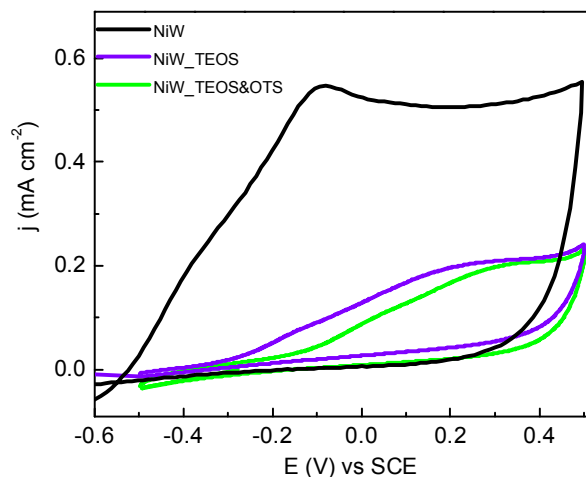
anodic process.



*Figure 7. Cyclic voltammograms of Ni–W and silanized samples at v: 0.025 V s$^{-1}$in still deaerated phosphate-borate buffer (0.1 M KH$_2$PO$_4$ + 0.05 M Na$_2$B$_4$O$_7$) pH 8.-100, with the addition of 1 M Na$_2$SO$_4$.*

Anodic polarization curves obtained at a low scan rate (2 mVs$^{-1}$) also give important

information on the corrosion behavior because under this condition $j \approx j_{corr}$ and $j_{ox} \approx 0$

(Figure 8). The analysis of these curves in comparison with those shown in Figure 7

indicates that TEOS inhibits oxide growth, while TEOS+OTS inhibits both oxide

growth and metal electrodissolution of the Ni–W coated steel. In fact, the blocking

effect of the polysiloxane layer is reflected by the lower $j_{corr}$ values recorded at a given

potential. Also, the potential at which the anodic dissolution process starts shifts to more

positive values in the presence of TEOS and TEOS & OTS coatings demonstrating their
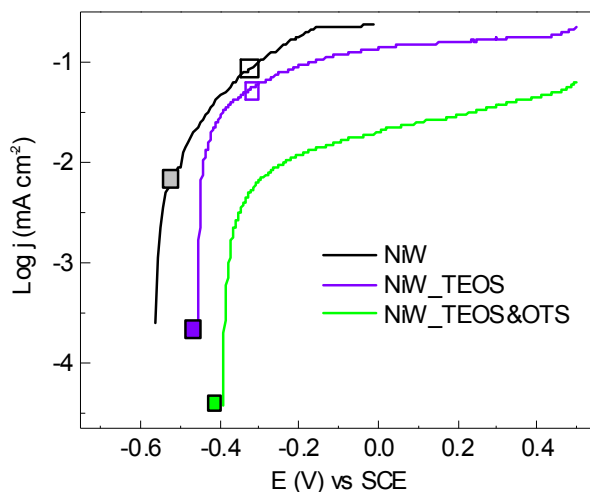
protective action.

14

*Figure 8. Anodic polarization curves at 2 mVs$^{-1}$ of Ni–W and silanized samples in still deaerated phosphate–borate buffer (0.1 M $KH_2PO_4$ + 0.05 M $Na_2B_4O_7$) pH 8.00, with the addition of 1 M $Na_2SO_4$. Empty squares symbols correspond to initial open circuit potentials (OCP) and color filled to final OCPs (see Figure 9)*

The effect of oxygen on the corrosion behavior was tested by measuring the open circuit potential (OCP) in a non-nitrogen bubbled electrolyte along the immersion time (Figure 9). It is evident that for both TEOS Ni–W and bare Ni–W coated steels, oxygen initially polarizes the systems to OCP values close to $\approx$ - 0.3 V, corresponding to high j (j $\approx$ 0.1 mA cm$^{-2}$, see Figure 8, empty square symbols). Then, they slowly decay to reach the values marked with filled squares in Figure 8. In contrast, OCP values of TEOS&OTS Ni–W coated steel remain stable along the immersion time indicating that oxygen is unable to induce the initial polarization of the sample. Also, note that the final OCP values for TEOS Ni–W and plain Ni–W coated samples have larger $j_{corr}$ values than the TEOS&OTS Ni–W coated steel (filled squares in Figure 8). Therefore, we can conclude that in the absence and in the presence of oxygen, the TEOS&OTS Ni–W coated steel exhibits a good corrosion resistance.
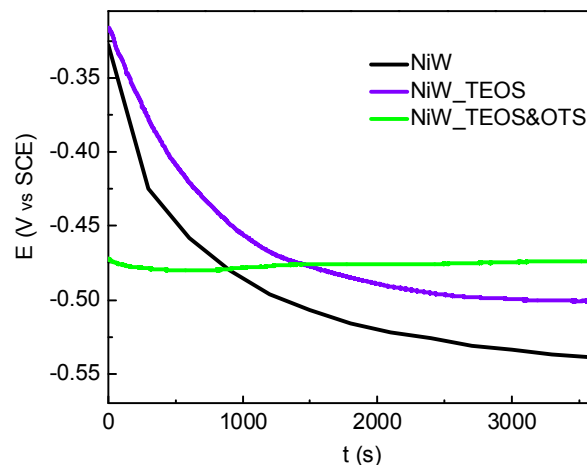
*Figure 9. Open circuit potential evolution of Ni–W and silanized samples in still phosphate-borate buffer (0.1 M KH$_2$PO$_4$ + 0.05 M Na$_2$B$_4$O$_7$) pH 8.00, with the addition of 1 M Na$_2$SO$_4$*

**Conclusions**

Electrodeposited nanostructured Ni–W coatings on carbon steel were functionalized by a two-step process involving tetraethoxysilane (TEOS) in combination with octadecyltrichlorosilane (OTS). We propose that TEOS reacts with the Ni–W oxidized surface providing a silica–rich surface suitable for further modification with OTS molecules. The silanized procedure forms a crystalline polysiloxane film that provides hydrophobicity and improves the corrosion behavior of the Ni–W surface coatings without modifying their excellent mechanical properties.

16

References

1       N. Eliaz, T. M. Sridhar and E. Gileadi, *Electrochim. Acta*, 2005, **50**, 2893-2904.
2       T. Yamasaki, P. Schloβmacher, K. Ehrlich and Y. Ogino, *Nanostruct. Mater.*, 1998, **10**, 375-388.
3       S. Lee, M. Choi, S. Park, H. Jung and B. Yoo, *Electrochim. Acta*, 2015, **153**, 225-231.
4       C. Borgia, T. Scharowsky, A. Furrer, C. Solenthaler and R. Spolenak, *Acta Mater.*, 2011, **59**, 386-399.
5       T. Yamasaki, *Mater. Phys. Mech.* , 2000, **1**, 127-132.
6       C. A. Schuh, T. G. Nieh and H. Iwasaki, *Acta Mater.*, 2003, **51**, 431-443.
7       A. R. Jones, J. Hamann, A. C. Lund and C. A. Schuh, *Plat. Surf. Finish.*, 2010, **97**, 52-60.
8       M. P. Quiroga Argañaraz, S. B. Ribotta, M. E. Folquer, L. M. Gassa, G. Benítez, M. E. Vela and R. C. Salvarezza, *Electrochim. Acta*, 2011, **56**, 5898-5903.
9       A. Chianpairot, G. Lothongkum, C. A. Schuh and Y. Boonyongmaneerat, *Corros. Sci.*, 2011, **53**, 1066-1071.
10      M. P. Q. Argañaraz, S. B. Ribotta, M. E. Folquer, E. Zelaya, C. Llorente, J. M. Ramallo-López, G. Benítez, A. Rubert, L. M. Gassa, M. E. Vela and R. C. Salvarezza, *Electrochim. Acta*, 2012, **72**, 87-93.
11      P. de Lima-Neto, A. N. Correia, R. A. C. Santana, R. P. Colares, E. B. Barros, P. N. S. Casciano and G. L. Vaz, *Electrochim. Acta*, 2010, **55**, 2078-2086.
12      M. A. Farzaneh, M. R. Zamanzad-Ghavidel, K. Raeissi, M. A. Golozar, A. Saatchi and S. Kabi, *Appl. Surf. Sci.*, 2011, **257**, 5919-5926.
13      W. Sassi, L. Dhouibi, P. Berçot, M. Rezrazi and E. Triki, *Appl. Surf. Sci.*, 2012, **263**, 373-381.
14      E. Navarro-Flores, Z. Chong and S. Omanovic, *J. Mol. Catal. A: Chem.*, 2005, **226**, 179-197.
15      M. Li, X. Wang, S. Li, S. Wang and X. Ma, *Int. J. Hydrogen Energy*, 2010, **35**, 6699-6708.
16      M. P. Quiroga Argañaraz, S. B. Ribotta, M. E. Folquer, G. Benítez, A. Rubert, L. M. Gassa, M. E. Vela and R. C. Salvarezza, *J. Solid State Electrochem.*, 2013, **17**, 307-313.
17      J. Sagiv, *J. Am. Chem. Soc.*, 1980, **102**, 92-98.
18      A. Ulman, *An Introduction to Ultrathin Organic Films: From Langmuir-Blodgett to Self-Assembly*, Academic Press, Boston, 1991.
19      A. Ulman, *Chem. Rev.*, 1996, **96**, 1533-1554.
20      J. J. Gooding and S. Ciampi, *Chem. Soc. Rev.*, 2011, **40**, 2704-2718.
21      R. Bhure and A. Mahapatro, *Silicon*, 2010, **2**, 117-151.
22      O. Azzaroni and R. C. Salvarezza, in *Supramolecular Chemistry: From Molecules to Nanomaterials.*, Ed. P. A. G. a. J. W. Steed, John Wiley & Sons, 2012, vol. 7, pp. 3445-3461.
23      R.-G. Hu, S. Zhang, J.-F. Bu, C.-J. Lin and G.-L. Song, *Prog. Org. Coat.*, 2012, **73**, 129-141.
24      W. van Ooij, D. Zhu, V. Palanivel, J. A. Lamar and M. Stacy, *Silicon Chem*, 2006, **3**, 11-30.
25      Z. Zhu, G. Xu, Y. An and C. He, *Colloids Surf., A*, 2014, **457**, 408-413.
26      E. Hoque, J. A. DeRose, P. Hoffmann, B. Bhushan and H. J. Mathieu, *J.Phys.Chem.C*, 2007, **111**, 3956-3962.

27      N. Metoki, L. Liu, E. Beilis, N. Eliaz and D. Mandler, *Langmuir*, 2014, **30**, 6791-6799.

28      G. Mani, M. D. Feldman, S. Oh and C. M. Agrawal, *Appl. Surf. Sci.*, 2009, **255**, 5961-5970.

29      R. Okner, G. Favaro, A. Radko, A. J. Domb and D. Mandler, *PCCP*, 2010, **12**, 15265-15273.

30      H. Ma, O. Acton, D. O. Hutchins, N. Cernetic and A. K. Y. Jen, *PCCP*, 2012, **14**, 14110-14126.

31      S. P. Pujari, L. Scheres, A. T. M. Marcelis and H. Zuilhof, *Angew. Chem. Int. Ed.*, 2014, **53**, 6322-6356.

32      A. Batan, N. Mine, B. Douhard, F. Brusciotti, I. De Graeve, J. Vereecken, M. Wenkin, M. Piens, H. Terryn, J. J. Pireaux and F. Reniers, *Chem. Phys. Lett.*, 2010, **493**, 107-112.

33      C. Haensch, S. Hoeppener and U. S. Schubert, *Chem. Soc. Rev.*, 2010, **39**, 2323-2334.

34      M. Cichomski, K. Kośla, J. Grobelny, W. Kozłowski, P. J. Kowalczyk, A. Busiakiewicz, W. Szmaja and J. Balcerski, *J. Alloys Compd.*, 2010, **507**, 273-278.

35      M. Cichomski and W. Szmaja, *Appl. Phys. A Mater. Sci.*, 2011, **102**, 339-343.

36      M. Cichomski, *Mater. Chem. Phys.*, 2012, **136**, 498-504.

37      M. Cichomski, K. Kośla, W. Pawlak, W. Kozłowski and W. Szmaja, *Tribol.Int.*, 2014, **77**, 1-6.

38      K. Kośla, J. Grobelny and M. Cichomski, *Appl. Surf. Sci.*, 2014, **314**, 500-504.

39      J. Feng, G. H. Xu, Y. An and X. Zeng, *Colloids Surf., A*, 2008, **316**, 194-201.

40      B. Arkles, Y. Pan, G. L. Larson and M. Singh, *Chem. Eur. J.*, 2014, **20**, 9442-9450.

41      S. H. Zaferani, M. Peikari, D. Zaarei, I. Danaee, J. M. Fakhraei and M. Mohammadi, *Corrosion*, 2013, **69**, 372-387.

42      V. Palanivel and W. J. Van Ooij, Modified silane coatings as an alternative to chromates for corrosion protection of aluminum alloys, in *Silanes and Other Coupling Agents, Vol. 3, pp.* , ed. K. L. Mittal, CRC Press, Taylor & Francis Group, 2004, vol. 3, pp. 135-159.

43      C. A. Acosta, R. C. Salvarezza, H. A. Videla and A. J. Arvia, *Corros. Sci.*, 1985, **25**, 291-303.

44      C. M. A. Brett and P. I. C. Melo, *J. Appl. Electrochem.*, 1997, **27**, 959-964.

45      R. Juškėnas, I. Valsiūnas, V. Pakštas and R. Giraitis, *Electrochim. Acta*, 2009, **54**, 2616-2620.

46      S. Meth and C. N. Sukenik, *Thin Solid Films*, 2003, **425**, 49-58.

47      I.-E. Bordianu, G. David, B. Simionescu, M. Aflori, C. Ursu, A. Coroaba, G. Hitruc, C. Cotofana and M. Olaru, *J.Mater.Chem.B*, 2015, **3**, 723-727.

48      R. C. Gray, J. C. Carver and D. M. Hercules, *J. Electron. Spectrosc. Relat. Phenom.*, 1976, **8**, 343-357.

49      D. Briggs and M. P. Seah Eds., *Practical Surface Analysis, Auger and X-ray Photoelectron Spectroscopy, Appendix 2:"Charge Referencing Techniques for Insulators"*, Wiley, London, 1990.

50      K. J. Kubiak, M. C. T. Wilson, T. G. Mathia and P. Carval, *Wear*, 2011, **271**, 523-528.

51      D. Ebert and B. Bhushan, *J. Colloid Interface Sci.*, 2012, **368**, 584-591.

52      B. Bhushan, M. Nosonovsky and Y. C. Jung, in *Nanotribology and Nanomechanics (Second Edition): An Introduction*, 2008, pp. 995-1072.

53      M. Nosonovsky and B. Bhushan, *Curr. Opin. Colloid Interface Sci.*, 2009, **14**, 270-280.

54      R. N. Wenzel, *Ind. Eng. Chem.*, 1936, **28**, 988-994.

55      A. B. D. Cassie and S. Baxter, *T.Faraday Soc.*, 1944, **40**, 546-551.

56      A. Y. Fadeev and T. J. McCarthy, *Langmuir*, 2000, **16**, 7268-7274.

57      G. Carson and S. Granick, *J. Appl. Polym. Sci.*, 1989, **37**, 2767-2772.

58      S. S. Latthe and A. L. Demirel, *Polym. Chem.*, 2013, **4**, 246-249.

59      Q. Zhang and L. A. Archer, *J.Phys.Chem.B*, 2003, **107**, 13123-13132.

60      R. G. Snyder, H. L. Strauss and C. A. Elliger, *J.Phys.Chem.*, 1982, **86**, 5145-5150.

61      D. L. Allara, A. N. Parikh and F. Rondelez, *Langmuir*, 1995, **11**, 2357-2360.

62      R. A. MacPhail, H. L. Strauss, R. G. Snyder and C. A. Elliger, *J.Phys.Chem.*, 1984, **88**, 334-341.

63      K. Kailasam, M. M. Natile, A. Glisenti and K. Müller, *J. Chromatogr. A*, 2009, **1216**, 2345-2354.

64      N. L. Jeon, K. Finnie, K. Branshaw and R. G. Nuzzo, *Langmuir*, 1997, **13**, 3382-3391.

65      A. N. Parikh, M. A. Schivley, E. Koo, K. Seshadri, D. Aurentz, K. Mueller and D. L. Allara, *J. Am. Chem. Soc.*, 1997, **119**, 3135-3143.

66      R. G. Snyder, *J.Chem.Phys.*, 1967, **47**, 1316-1360.

67      A. N. Parikh, B. Liedberg, S. V. Atre, M. Ho and D. L. Allara, *J.Phys.Chem.*, 1995, **99**, 9996-10008.

68      R. Wang, G. Baran and S. L. Wunder, *Langmuir*, 2000, **16**, 6298-6305.

69      O. P. Khatri and S. K. Biswas, *Surf. Sci.*, 2004, **572**, 228-238.

70      A. Flores, F. Ania and F. J. Baltá-Calleja, *Polymer*, 2009, **50**, 729-746.